第37卷第1期 无 机 化 学 学 报 Vol.37 No.1
2021年1月 CHINESE JOURNAL OF INORGANIC CHEMISTRY 131-139

超微$Ni(OH)_2$纳米粒子的合成及其对Li^+的超高吸附性能

景 楠[1] 周安南[1] 王国会[1] 王润伟[2] 徐庆红*,[1]
([1]北京化工大学,化工资源有效利用国家重点实验室,北京 100029)
([2]吉林大学化学学院,无机合成与制备化学国家重点实验室,长春 130012)

摘要: 在葡萄糖水溶液中合成得到平均粒径为5 nm的α-$Ni(OH)_2$超微纳米粒子。研究结果发现,在水溶液中葡萄糖浓度能够控制α-$Ni(OH)_2$纳米粒子粒径的大小,我们对其中的原理进行了剖析。当没有葡萄糖存在时,合成得到的$Ni(OH)_2$晶型为β型,且颗粒粒径尺寸分布为微米级别。另外,研究发现α-$Ni(OH)_2$超微纳米粒子室温下对中性水溶液中Li^+具有较强的吸附性能,且这种吸附性能随粒径的减小而剧烈增大;粒径为5 nm的α-$Ni(OH)_2$粒子对Li^+的最大吸附量为214 $mg\cdot g^{-1}$(远大于文献报道的有关吸附剂对Li^+的吸附容量),而粒径为1 μm的β-$Ni(OH)_2$在相同条件下对Li^+的最大吸附量低于30 $mg\cdot g^{-1}$。计算分析表明,Li^+在α-$Ni(OH)_2$纳米粒子表面吸附满足Freundlich方程,符合层层吸附模型。

关键词: $Ni(OH)_2$; 超微纳米粒子; Li^+离子; 吸附
中图分类号: O647.3 **文献标识码:** A **文章编号:** 1001-4861(2021)01-0131-09
DOI: 10.11862/CJIC.2021.015

$Ni(OH)_2$ with Super-Small Nanoscale: Synthesis and Application in Li^+ Adsorptions

JING Nan[1] ZHOU An-Nan[1] WANG Guo-Hui[1] WANG Run-Wei[2] XU Qing-Hong*,[1]
([1]*State Key Laboratory of Chemical Resource Engineering, Beijing University of Chemical Technology, Beijing* 100029, *China*)
([2]*State Key Laboratory of Inorganic Synthesis and Preparative Chemistry, College of Chemistry, Jilin University, Changchun* 130012, *China*)

Abstract: α-$Ni(OH)_2$ nanoparticles with 5 nm average diameter were prepared under the existence of glucose in water solution, and the size of α-$Ni(OH)_2$ nanoparticles was found to be controlled by the concentration of glucose. A possible mechanism of the preparation process was proposed. When the synthesis was processed without existence of the glucose, β-$Ni(OH)_2$ was obtained. The super-small α-$Ni(OH)_2$ nanoparticles showed strong adsorption ability to Li^+ ions when pH value of the solution was about 7.0 under room temperature. Maximum adsorption capacity of the super-small α-$Ni(OH)_2$ nanoparticles to Li^+ was about 214 $mg\cdot g^{-1}$; however, the β-$Ni(OH)_2$ with diameter above 1.0 μm was low than 30 $mg\cdot g^{-1}$. Freundlich equation analysis and SEM images of the adsorption products indicate multilayers′ adsorption process to Li^+ of α-$Ni(OH)_2$ nanoparticles.

Keywords: nickel hydroxide; super-small nanoparticle; lithium ion; adsorption

With the development of microelectronics technology, the integration, miniaturization and intelligent of mobile equipment require that the battery has high efficiency and light weight. Due to non-pollution, high cycle life, high working voltage, light weight and rapid charging[1-5], lithium ion battery has promising prospect in our daily life. However, how to extract Li^+ ion from ocean has been bothering many scientists for many years, for low concentration of Li^+ in ocean[6]. Adsorption is one of a simple and low-cost method for Li^+

收稿日期:2020-02-28。收修改稿日期:2020-11-09。
国家自然科学基金(No.21521005,U1362113)和吉林大学无机水热合成与制备化学国家重点实验室开放课题(2018)资助。
*通信联系人。E-mail:xuqh@mail.buct.edu.cn

enrichment. Sieve[7-10] and grapheme[11-15] are often used as traditional adsorbents to Li^+.

Nickel hydroxide ($Ni(OH)_2$), a kind of transition metal hydroxide, has excellent electrochemical performance[16]. Due to high surface area and chemical activity, $Ni(OH)_2$ with nanoscale was also used as catalyst, such as oxidative degradation of phenolic pollutants[17], hydrogenation reduction of nitrophenol[18]. Traditional nano $Ni(OH)_2$ preparation methods, such as hydrothermal method[19-21], chemical precipitation method[22] and sonochemical method[23-25], usually need rigorous reaction conditions, which result in high cost and energy use, and super-small $Ni(OH)_2$ nanoparticles (<10 nm) are hardly obtained.

In 2000, Nauta found that some extraneous water molecules could enter and exist in the water cluster in liquid helium (Fig. S1A, Supporting information) [26]. Later, Cheng proved that the distribution of ethanol and water molecules were not randomly in their mixed system (Fig.S1B)[27]. When concentration of ethanol was high, water molecules were separated into tiny agglomerates by ethanol molecules under the function of hydrogen bonds, and no isolated water molecule could be found in the system. According to the upon ideas, we pointed out "molecular cage" concept relating to the restrict area synthesis in our previous work[28-29], and molecules of glucose were used to build relatively stable "molecular cage". In glucose solution, hydrogen bonds can be easily formed among glucose and water molecules. Once the concentration of glucose reaches a high level, water molecules will be surrounded by the "cage" (Fig. S2), and some materials with super-small nanoscale can be synthesized in the cages.

In this work, the α-$Ni(OH)_2$ nanoparticles with 5 nm average diameter was successfully prepared by the reaction between NaOH and $LiNO_3$ under the existence of glucose in water solution, and the size of α-$Ni(OH)_2$ nanoparticles was found to be controlled by the concentration of glucose (Fig. 1). However, β-$Ni(OH)_2$ with large scale was obtained when the synthesis was processed without glucose. The preparation on α-$Ni(OH)_2$ super-small nanoparticles is easily to be realized and has environmental friendship property.

As it is known that the $Ni(OH)_2$ with large scale almost has no adsorption ability to Li^+ ions, however, the α-$Ni(OH)_2$ with super-small nanoscale has strong adsorption ability to Li^+ when the pH value of solution is about 7.0 under room temperature. Maximum adsorption capacity of the nanoparticles to Li^+ was about 214 $mg\cdot g^{-1}$, much larger than that of β-$Ni(OH)_2$ with diameter of 1.0 μm (low than 30 $mg\cdot g^{-1}$).

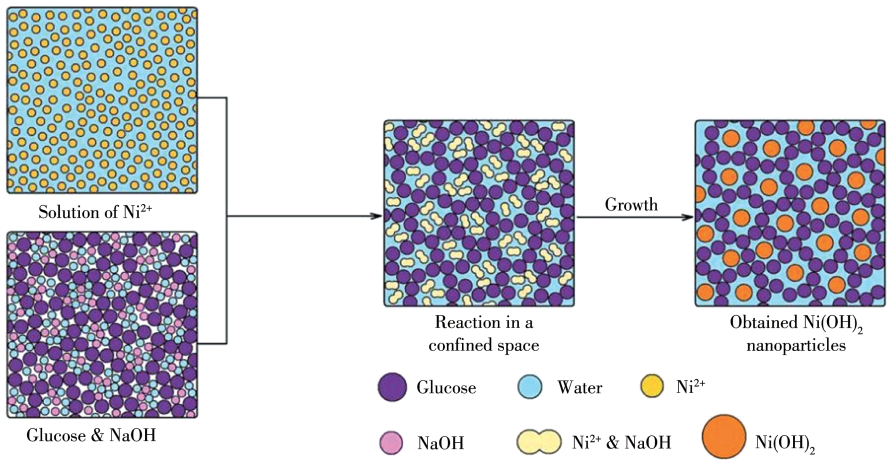

Fig.1 Formation process of super-small $Ni(OH)_2$ nanoparticles

1 Experimental

1.1 Materials and chemicals

Glucose, $Ni(NO_3)_2$, NaOH and $LiNO_3$ were purchased from Beijing Chemical Reagent Company (Beijing, China). All chemicals are analytical grade and used without further purification. Deionized water was used throughout the experiments.

1.2 Characterization

Nicolet 8700 Fourier transform infrared spectrometer (FTIR, Thermo Electron, USA) was used to characterize the functional groups of $Ni(OH)_2$ samples before and after adsorption. FTIR spectra were acquired at a resolution of 4 cm^{-1} in a wave number range from 4 000 to 400 cm^{-1} with 32 co-added scans for the samples and background. X-ray diffraction (XRD) patterns of the samples were measured on a DX-1000 X-ray diffractometer with Cu $K\alpha$ radiation (λ=0.154 06 nm) from 5° to 90° with a scanning rate of 10°·min^{-1}, and the working accelerating voltage and emission current were 40 kV and 40 mA, respectively. S-4700 field emission scanning electron microscope (SEM, Hitachi, Japan) operated at 15 kV and J-3010 high resolution transmission electron microscopy (HRTEM, Hitachi J-3010, Japan) operated at 200 kV were used to observe the morphologies of synthesized $Ni(OH)_2$ nanoparticles. The iCAP 6300 inductively coupled plasma optical atomic emission spectrometry (ICP-OES, Thermo Electron, USA) was used to investigate Li^+ concentration in the solution after adsorption, and the power of ICP-OES was 1 500 W and the pump speed was 50 r·min^{-1}. The auxiliary gas flow and atomized gas flow were 1.5 L·min^{-1}, and the cooling air flow was 12 L·min^{-1}. N_2 adsorption-desorption isotherms were recorded on a Quantachrome NOVA 2000e sorption analyzer at the temperature of liquid nitrogen (77 K). The sample was degassed at 150 ℃ overnight prior to the measurement. The surface area was obtained by the Brunauer-Emmett-Teller (BET) method.

1.3 Preparation of $Ni(OH)_2$ nanoparticles

A certain amount of glucose (0, 5, 10 and 20 g) and 1 g of NaOH were dissolved in 100 mL of deionized water. 100 mL of $Ni(NO_3)_2$ (0.01 mol·L^{-1}) solution was then added dropwise into the above glucose alkaline solution, and the $Ni(OH)_2$ nanoparticle formed immediately. The products were noted as Ni-0, Ni-5, Ni-10 and Ni-20, respectively. The synthesized $Ni(OH)_2$ nanoparticles were separated by high-speed centrifugation (10 000 r·min^{-1} for 15 min) and washed with deionized water for several times to remove glucose, NaOH and other unreacted raw materials.

1.4 Adsorptions of Li^+ ions

A certain amount of $LiNO_3$ (from 0.02 to 1.5 g) was dissolved with 1 L of deionized water to obtain the solutions with different concentrations (from 20 to 1 500 mg·L^{-1}) of Li^+. The adsorption kinetics for Li^+ on the surface of $Ni(OH)_2$ nanoparticles was obtained from a series of experiments by dispersing 0.2 g of Ni-20 sample into 200 mL Li^+ aqueous solution. The effect of temperature (from 20 to 80 ℃) was studied with the initial concentration of Li^+ at 80 mg·L^{-1} and the contact time of 0.5 h. The effect of contact time (from 10 min to 6 h) on the adsorption process was investigated with the initial concentration of Li^+ at 80 mg·L^{-1} under 20 ℃. The adsorption effect of concentration (from 20 to 1 500 mg·L^{-1}) of Li^+ was studied at 20 ℃ for 2 h. The mixtures after adsorption were centrifugated (10 000 r·min^{-1} for 15 min) and the supernates were characterized by ICP test to investigate the concentrations of residual Li^+ ions. The sample Ni-0 synthesized was used to repeat the above process for a contrast. The adsorption capacity (q_e, mg·g^{-1}) was calculated with the following equation (**1**): $q_e=(c_0-c_e)V/m$, where c_0 and c_e are the initial and equilibrium concentrations (mg·L^{-1}) of Li^+ ions, m is the mass of the adsorbent (g), V is the volume of the solution (L).

In addition, the selection adsorptions of Ni-20 to Li^+, Na^+ and K^+ were checked. 0.2 g of Ni-20 sample was dispersed into 200 mL neutral solution containing Li^+ (1 500 mg·L^{-1}), Na^+ (1 500 mg·L^{-1}), K^+ (1 500 mg·L^{-1}) and Mg^{2+} (1 500 mg·L^{-1}) ions, and the mixture was stirred for 2 h at 20 ℃. The other experimental conditions were same as the formers.

2 Results and discussion

2.1 Characterizations for $Ni(OH)_2$ particles

FTIR spectra of the $Ni(OH)_2$ particles synthesized with and without existence of glucose were studied, which are shown in Fig. 2. The product has standard absorption of β-$Ni(OH)_2$ when no glucose was added during the preparation (Fig. 2A), and absorptions of stretching vibration of OH^- in the product appeared at 3 639 cm^{-1}. However, the spectra of the products synthesized under the existence of glucose had characteris-

tic of α-$Ni(OH)_2$ (Fig. 2B), and the absorptions of OH^- in the products were found at 3 423 cm^{-1}. The above results indicate that the crystalline form of $Ni(OH)_2$ synthesized changed from β to α type when glucose was added in the preparation.

Fig. 3 shows the XRD patterns of $Ni(OH)_2$ products. When no glucose was added during the preparation (Fig. 3A), the diffractions from (001), (100), (101), (102), (110) and (111) planes of synthesized $Ni(OH)_2$ were found at 17.9°, 33.2°, 38.6°, 51.8°, 59.2° and 62.8°, respectively, which coincide with the standard XRD data of β-$Ni(OH)_2$. However, when glucose was added in the preparation, XRD patterns of the $Ni(OH)_2$ products had obvious difference from Ni-0, and weak diffractions from (003), (101) and (110) planes of the products were located at 11.7°, 34.0° and 80.1°, respectively, which are contributed to the standard XRD pattern of α-$Ni(OH)_2$. However, the crystallinities of these samples are low. The XRD results also proves the change of crystalline form of $Ni(OH)_2$ particles with the glucose being added or not in preparation.

SEM images (Fig.4) show that the morphologies of $Ni(OH)_2$ products have obvious differences among Ni-0, Ni-5, Ni-10 and Ni-20. 200 particles of Ni-10 and Ni-20 were chosen randomly to obtain the relevant statistical particle size. Ni-0 shows irregular bulk morphology (Fig.4A), and there is only simple ionic reaction between Ni^{2+} and OH^- when no glucose was added in the preparation. The morphology of Ni-5 (5 g of glucose was added, Fig.4B) has obvious change comparing with Ni-0, and some globular particles in the product appeared. The particle size distribution in Ni-5 was difficult to evaluate for the serious agglomeration. When the amount of added glucose was increased to 10 g in the preparation, the product (Ni-10) had irregular small particle morphology (Fig.4C) and its diameter distribution ranged from 10 to 190 nm with an average value of 70 nm. When the amount of added glucose was increased to 20 g in the reaction, the product (Ni-20) had super-small globular morphology, and diameter distribution of the particles ranged from 3 to 8 nm with an average value of 5 nm (Fig.4D), further smaller than

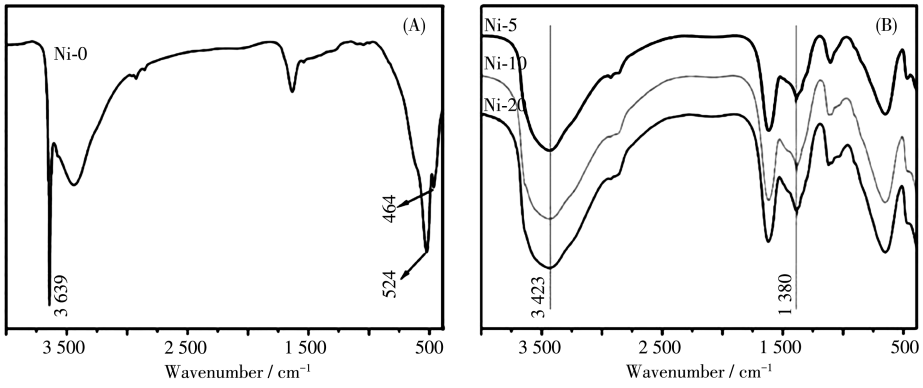

Fig.2 FTIR spectra of $Ni(OH)_2$ nanoparticles prepared with various glucose concentrations

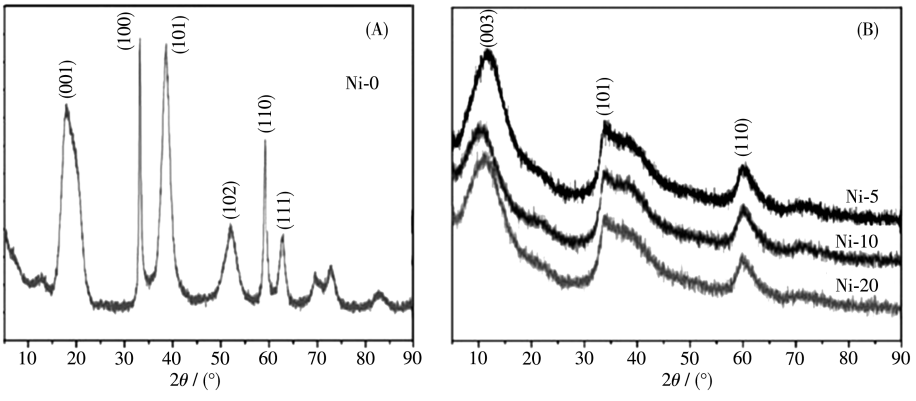

Fig.3 XRD patterns of $Ni(OH)_2$ nanoparticles prepared with various glucose concentrations

those of Ni-5 and Ni-10. That is to say, a few "restricted areas" were formed when little glucose was added, and the regular small α-$Ni(OH)_2$ nanoparticles were difficult to obtained. On the contrary, the number of "restricted area" was increased with the increasing amount of added glucose and the size and morphology of α-$Ni(OH)_2$ were controlled by the limitation domain effect. All the reactions between Ni^{2+} and OH^- happened in the areas when the number of "restricted area" reached saturation. Moreover, the BET analysis shows that the surface area of synthesized Ni-20 nanoparticles was about 101 $m^2 \cdot g^{-1}$ while Ni-0 was only 29 $m^2 \cdot g^{-1}$.

Fig.5 shows the HRTEM images of Ni-5, Ni-10 and Ni-20. When 5 g of glucose was added in the reaction (Fig.5A), Ni-5 showed irregular bulk morphology and the corresponding particle size of the product was about 200 nm. When the amount of added glucose was increased to 10 g (Fig.5B), the size of α-$Ni(OH)_2$ particle was obvious smaller than Ni-5, but its morphology was still irregularity. However, when the additive amount of glucose was further increased to 20 g (Fig.5C), almost all α-$Ni(OH)_2$ particles showed supersmall size and the diameters of these particles were smaller than 10 nm. The HRTEM results are consistent with SEM results.

Restricted area (or molecular cage) effect of glucose in water solution possibly plays an important role in the synthesis. Some restricted areas will be formed by the hydrogen bonds among glucose molecules, for existence of hydroxyls in the molecules. The restricted area will be difficult to be formed when concentration of glucose is low in the solution, and the opposite case will appear when concentration of glucose is high. In a glucose solution with high concentration, the reactions between Ni^{2+} and OH^- will be restricted in the molecular cages and $Ni(OH)_2$ particles with small diameters will be obtained. This synthetic effect of molecular cage is more and more evident with increase of glucose concentration until numbers of the cages reach satura-

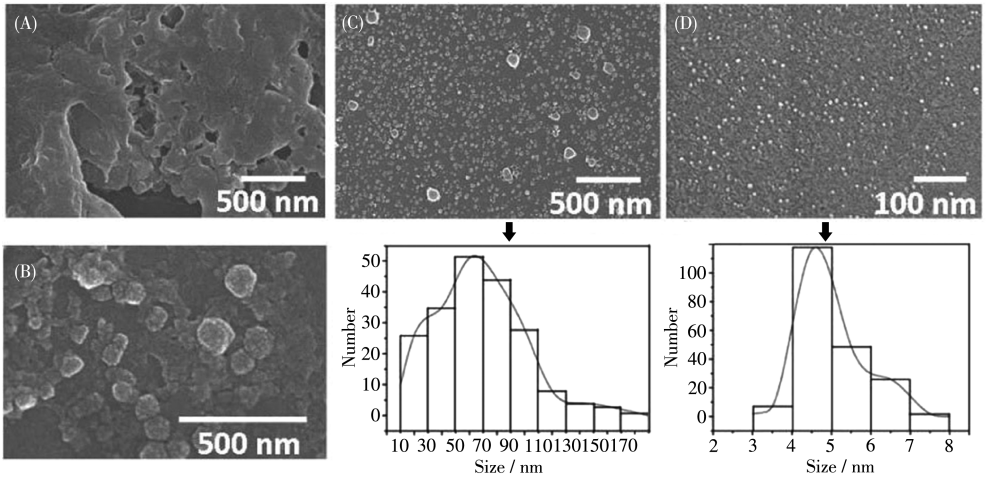

Fig.4　SEM images and the corresponding statistical particle size results of $Ni(OH)_2$ prepared with various glucose concentrations: Ni-0 (A), Ni-5 (B), Ni-10 (C) and Ni-20 (D)

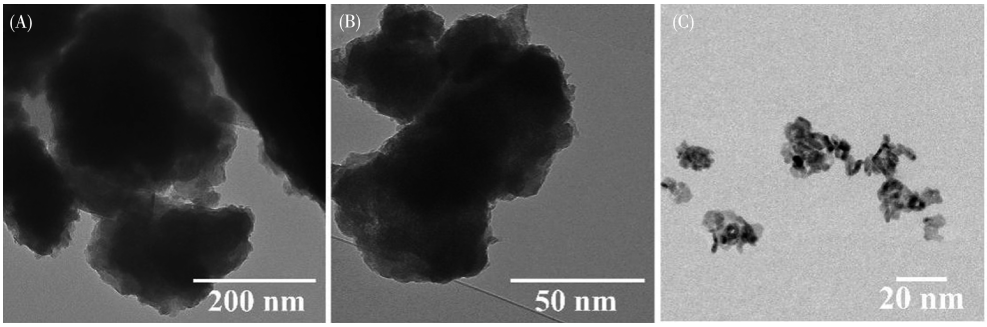

Fig.5　HRTEM images of α-$Ni(OH)_2$ prepared with various glucose concentrations: Ni-5 (A), Ni-10 (B) and Ni-20 (C)

tion. Thus, $Ni(OH)_2$ with super-small globular scale and narrow distribution in size was finally synthesized.

2.2 Adsorptions on super-small $Ni(OH)_2$ nanoparticles to Li^+ ions

The sample Ni-20 was chosen to study the adsorption ability of α-$Ni(OH)_2$ to Li^+ ions, and Ni-0 was used for a comparison. Fig.6 shows that the adsorption effects of Ni-20 and Ni-0 with contact time from 10 min to 6 h while the initial concentration of Li^+ was 80 $mg\cdot L^{-1}$ and the temperature during the adsorption process was at 20 ℃. The result shows that the adsorption capacity of Ni-0 was lower than 10 $mg\cdot g^{-1}$ after 6 h, indicating a low adsorption of bulk β-$Ni(OH)_2$ to Li^+ ions. However, the adsorption capacity of Ni-20 was about 23 $mg\cdot g^{-1}$ under the same conditions.

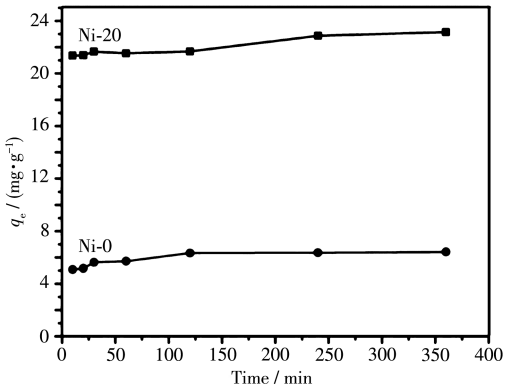

Fig.6 Effect of contact time (10, 20, 30 min, 1, 2, 4 and 6 h) on adsorption capacity for Ni-0 and Ni-20

The temperature effects on adsorption process of Ni-20 and Ni-0 to Li^+ at the initial concentration of 80 $mg\cdot L^{-1}$ in 30 min are shown in Fig.7. With increase of the temperature, the adsorption capacities of both Ni-20 and Ni-0 increased slowly and Ni-20 showed better adsorption abilities than those of Ni-0 at any temperatures. Improvement on adsorption performance of $Ni(OH)_2$ by increasing of temperature has a little affect.

Adsorption isotherm studies are important to determine the efficacy of adsorbent. The adsorption isotherms of Ni-20 and Ni-0 were investigated by varying Li^+ concentration from 20 to 1 500 $mg\cdot L^{-1}$ when the other conditions was T=20 ℃, contact time=2 h and pH =7.0 (Fig.8). For Ni-0, even when the initial concentration of Li^+ increased to 1 500 $mg\cdot L^{-1}$, the adsorption capacity was still low than 30 $mg\cdot g^{-1}$, showing poor

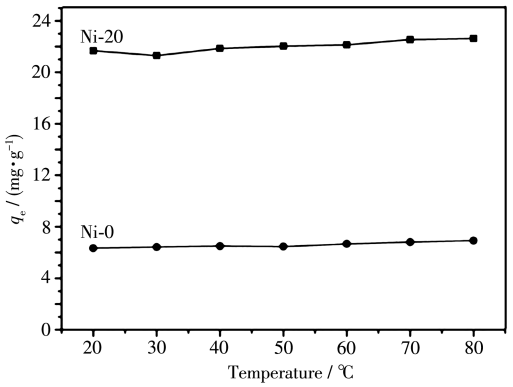

Fig.7 Effect of temperature (20, 30, 40, 50, 60, 70 and 80 ℃) on adsorption capacity for Ni-0 and Ni-20

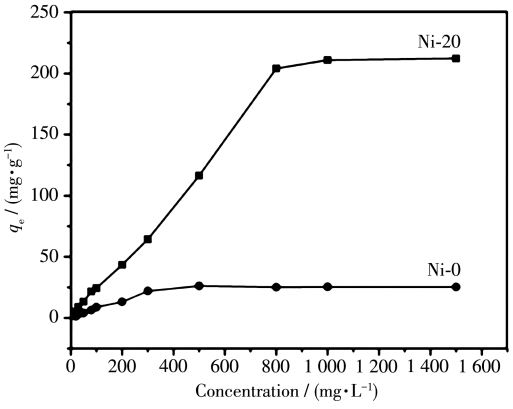

Fig.8 Effect of initial metal concentration (from 20 to 1 500 $mg\cdot L^{-1}$) on adsorption capacity for Ni-20

adsorption performance to Li^+. However, the largest adsorption capacity of Ni-20 was near to 214 $mg\cdot g^{-1}$, showing excellent adsorption ability. The largest adsorption capacities of Ni-10 and Ni-5 were about 107 and 63 $mg\cdot g^{-1}$ under the conditions, respectively. The above results indicate that the significant influence from size effect of the samples on the adsorption performance.

On the other hand, many differences on the adsorption ability of super-small α-$Ni(OH)_2$ nanoparticles to different alkali metal ions were found. The largest adsorption capacities of Ni-20 to Li^+, Na^+ and K^+ were 152, 43 and 19 $mg\cdot g^{-1}$, respectively, when 0.2 g of Ni-20 was dispersed in a neutral solution containing Li^+ (1 500 $mg\cdot L^{-1}$), Na^+ (1 500 $mg\cdot L^{-1}$) and K^+ ions (1 500 $mg\cdot L^{-1}$) for 2 h at 20 ℃. However, when the mixture contained Mg^{2+} ions (1 500 $mg\cdot L^{-1}$), the largest adsorption capacities of Ni-20 to the four ions were 73 $mg\cdot g^{-1}$ (Li^+), 35 $mg\cdot g^{-1}$ (Na^+), 14 $mg\cdot g^{-1}$ (K^+) and 84

$mg\cdot g^{-1}$ (Mg^{2+}) under the same conditions as former. The adsorbent has selective adsorption among Li^+, Na^+ and K^+ ions, but not to Mg^{2+} ion. The reason on the difference possibly come from different diameters and valences of the metal ions, diameters of Li^+, Na^+, K^+ and Mg^{2+} are 76, 102, 138 and 72 pm, respectively, and valence of Mg^{2+} is larger than the others.

2.3 Discussion on the mechanism of adsorption

Langmuir and Freundlich adsorption models were used to investigate the adsorption behaviors of Ni-20 to Li^+. Langmuir equation is expressed as follow:

$$\frac{c_e}{q_e}=\frac{1}{Q_{max}K}+\frac{c_e}{Q_{max}} \quad (2)$$

Where q_e is the equilibrium adsorption capacity ($mg\cdot g^{-1}$), c_e is the equilibrium concentration ($mg\cdot L^{-1}$) of metallic ion, Q_{max} is the max adsorption capacity, K is the Langmuir constant which is relative to the adsorption ability.

Freundlich equation is expressed as follow:

$$\ln q_e=\ln K_f+\frac{1}{n}\ln c_e \quad (3)$$

Where q_e is the equilibrium adsorption capacity, c_e is the equilibrium concentration ($mg\cdot L^{-1}$) of metal ion, K_f and n are the Freundlich model constants that can be determined by plotting $\ln q_e$ versus $\ln c_e$.

Fig. 9A indicates that a linear plot cannot be obtained when c_e/q_e was plotted against c_e (the corresponding R^2 was only 0.679 6). That is to say, Langmuir model is not suitable to describe the adsorption process. On the contrary, a linear plot could be obtained when $\ln q_e$ was plotted against $\ln c_e$ (Fig.9B, the corresponding R^2 was 0.982 1), suggesting the adsorption accords with Freundlich model and the adsorption has a multilayer adsorption process.

SEM and FTIR were used to investigate the change on structures of Ni-20 after adsorption (Fig.10). The size of adsorbents after the adsorption had significant increase with the increase of initial concentration of Li^+. When initial concentration of Li^+ was 20 $mg\cdot L^{-1}$ (Fig.10A), the size and morphology of adsorption product was similar to the original particles for a low adsorption capacity. With the increase of initial Li^+ concentration, the size of adsorbent after adsorption had obvious increase. Meanwhile, some aggregates appeared in the cases.

FTIR spectra of the adsorption products were similar to that of Ni-20 when initial concentrations of Li^+ were low (Fig. 10A~10D). While when the initial concentration of Li^+ was more than 100 $mg\cdot L^{-1}$ (Fig.10E~10H), the adsorption of NO_3^- at 1 380 cm^{-1} became stronger, indicating more NO_3^- ions were adsorbed simultaneously and $LiNO_3$ possibly formed in the layer-by-layer adsorption process. However, $LiNO_3$ forming on the surface of adsorbent did not dissolve again in the solutions with high concentrations of Li^+.

The multilayer adsorption in this study can be explained. Due to the existence of large number of OH^- groups on the surface of α-$Ni(OH)_2$ nanoparticles and super small in size, the surface polarity of the nanoparticles is very strong. At the very beginning, some NO_3^- groups are stabled on the surface of nanoparticles by hydrogen bonds for the existence of OH^- in $Ni(OH)_2$. At the same time, some Li^+ ions are embedded in the gaps of adsorbed NO_3^- groups to balance the electronegativity from nitrate, then a uniform adsorption layer of NO_3^- groups and Li^+ ions is thus formed on the nanoparticle

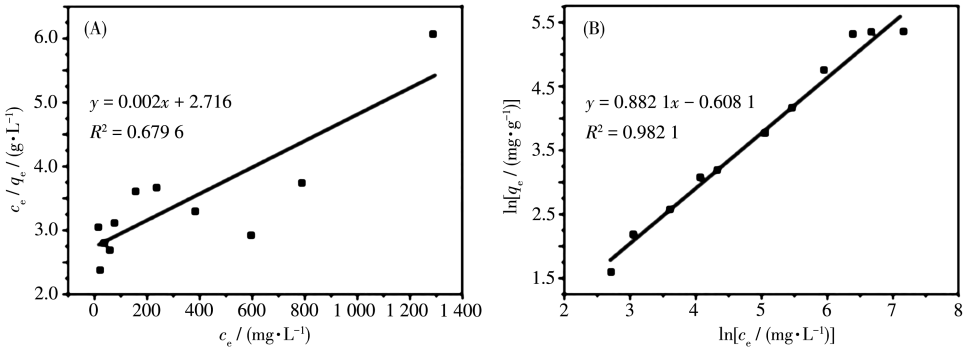

Fig.9　Results of Langmuir (A) and Freundlich (B) adsorption model analysis

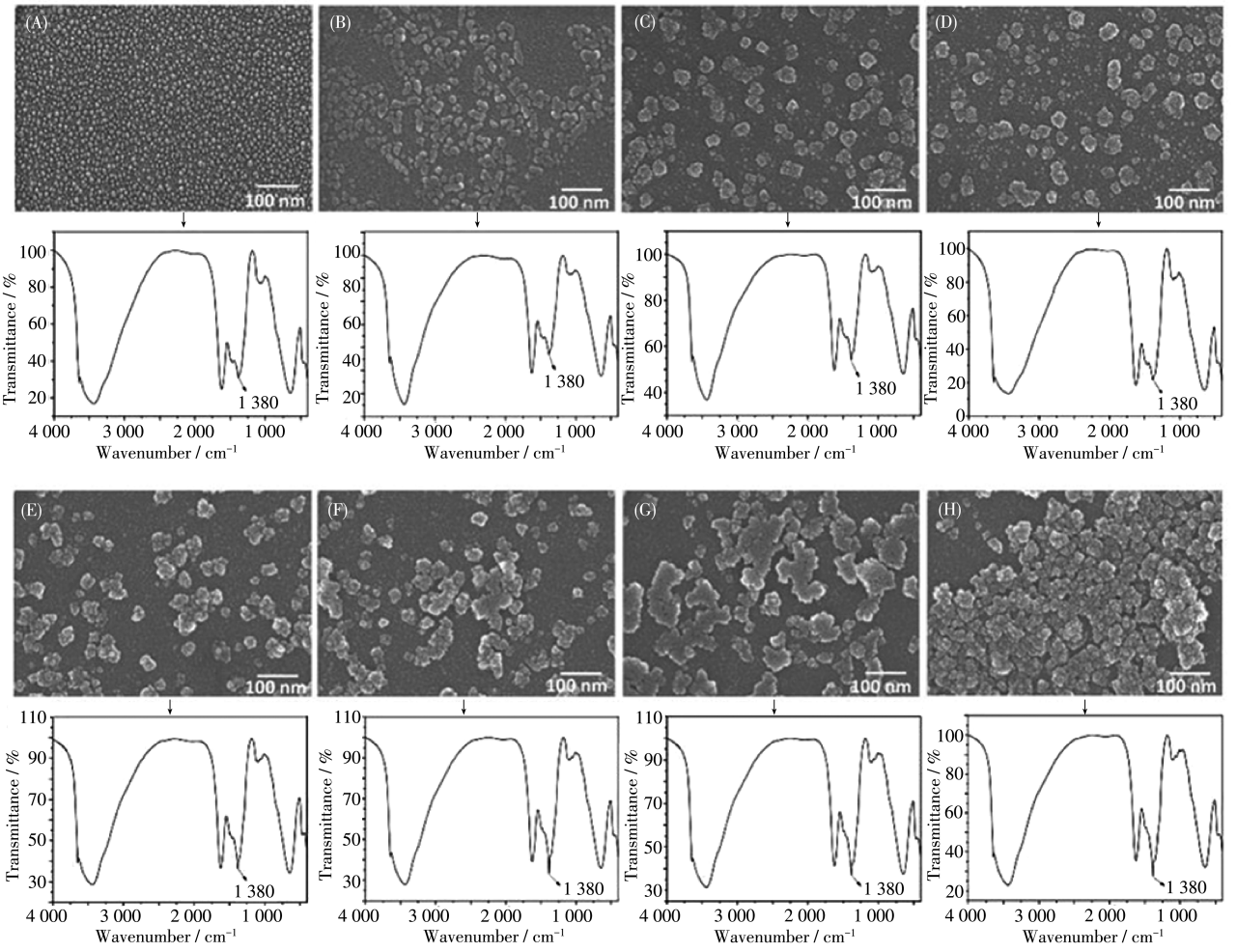

Fig.10 SEM and FTIR results of Ni-20 after adsorbed Li^+ with different initial concentration: 20 mg·L^{-1} (A), 50 mg·L^{-1} (B), 80 mg·L^{-1} (C), 100 mg·L^{-1} (D), 300 mg·L^{-1} (E), 500 mg·L^{-1} (F), 800 mg·L^{-1} (G) and 1 000 mg·L^{-1} (H)

surface. Later, Li^+ ions and NO_3^- groups are adsorbed continually for the electronegativity of NO_3^- and the positivity of Li^+ adsorbed previously, and a multilayer adsorption is thus formed. Under the strong actions among the ions adsorbed and ions to the adsorbent, the NO_3^- and Li^+ ions adsorbed could not be dissolved again. This is the reason why the particle size of $Ni(OH)_2$ nanoparticles as adsorbents increases dramatically after adsorption.

3 Conclusions

A "molecular confinement" method was used to prepare super-small α-$Ni(OH)_2$ nanoparticles with average diameter of 5 nm in this work. The α-$Ni(OH)_2$ nanoparticles were used adsorbents to adsorb Li^+ from water. Compared with traditional bulk β-$Ni(OH)_2$ that had a little adsorption to Li^+, the adsorption ability of super-small α-$Ni(OH)_2$ nanoparticles had obvious improvement and its largest adsorption capacity was near to 214 mg·g^{-1} in high concentration solution of Li^+. Further studies indicate that the adsorption obeys the Freundlich mode, and $LiNO_3$ is possibly formed simultaneously on surface of the adsorbent during adsorption process.

Acknowledgements: We thank associate professor ZHANG Pu-Dun for his advice.

Supporting information is available at http://www.wjhxxb.cn

References:

[1] Park J, Park S S, Won Y S. *Electrochim. Acta*, **2013**,**107**:467-472

[2] Yan L, Yu H X, Qian S S, Li P, Lin X T, Long N B, Zhang R F, Shui M, Shu J. *Electrochim. Acta*, **2016**,**213**:217-224

[3] Li X, Lin H C, Cui W J, Xiao Q, Zhao J B. *ACS Appl. Mater. Interfaces*, **2014**,**6**:7895-7901

[4] Wang Y, Rong H B, Li B Z, Xing L D, Li X P, Li W S. *J. Power Sources*, **2014**,**246**:213-218

[5] Long D H, Jeong M G, Lee Y S, Choi W, Lee J K, Oh I H, Jung H G. *ACS Appl. Mater. Interfaces*, **2015**,**7**:10250-10257

[6] Choubey P K, Chung K S, Kim M S, Lee J C, Srivastave R R. *Miner. Eng.*, **2017**,**110**:104-121

[7] Ma L W, Nie Z R, Xi X L, Zhao L Y, Chen B Z. *J. Environ. Chem. Eng.*, **2017**,**5**:995-1003

[8] Wang S L, Li P, Cui W W, Zhang H L, Wang H Y, Zheng S L, Zhang Y. *RSC Adv.*, **2016**,**6**:102608-102616

[9] Xiao G P, Tong K F, Zhou L S, Xiao J L, Sun S Y, Li P, Yu J G. *Ind. Eng. Chem. Res.*, **2012**,**51**:10921-10929

[10]Chen M M, Wu R Y, Ju S G, Zhang X X, Xue F, Xing W H. *Microporous Mesoporous Mater.*, **2018**,**261**:29-34

[11]Sun S, Chen L Y, Sun H L, Zhang T Y. *Electrochim. Acta*, **2018**,**259**:1089-1094

[12]Fan X F, Zheng W T, Kuo J L. *ACS Appl. Mater. Interfaces*, **2012**,**4**:2432-2438

[13]Fan X F, Zheng W T, Kuo J L, Singh D J. *ACS Appl. Mater. Interfaces*, **2013**,**5**:7793-7797

[14]Yildirim H, Kinaci A, Zhao Z J, Chan M K Y, Greeley J P. *ACS Appl. Mater. Interfaces*, **2014**,**6**:21141-21150

[15]Koh W, Lee J H, Lee S G., Choi J I, Jang S S. *RSC Adv.*, **2015**,**5**:32819-32825

[16]Li H, Ding Y C, Yuan J L, Wang Z Y. *J. Power Sources*, **1995**,**57**(57):137-140

[17]Saeed M, Ilyas M. *Appl. Catal. B*, **2013**,**129**:247-254

[18]Jiang Z F, Xie J M, Jiang D L, Wei X J, Chen M. *CrystEngComm*, **2013**,**15**:560-569

[19]Jiang C, Zhao B, Cheng J Y, Li J Q, Zhang H J, Tang Z H, Yang J H. *Electrochim. Acta*, **2015**,**173**:399-407

[20]Xiao Q, Wang X X, Huang S P. *Mater. Lett.*, **2017**,**198**:19-22

[21]Wang H Z, Shi X, Zhang W G, Yao S W. *J. Alloys Compd.*, **2017**,**711**:643-651

[22]Wang T, Pan J Q, Achille K G, Sun Y Z. *Int. J. Hydrogen Energy*, **2017**,**42**:19139-19147

[23]Numan A, Duraisamy N, Omar F S, Gopi D, Ramesh K, Ramesh S. *Prog. Nat. Sci.*, **2017**,**4**:416-423

[24]Vidotti M, Van Greco C, Ponzio E A, Cordoba de Torresi S I. *Electrochem. Commun.*, **2006**,**8**:554-560

[25]Abbasian H, Ghanbari D. *Physica E*, **2015**,**65**:106-109

[26]Nauta K, Miller R E. *Science*, **2000**,**287**:293-295

[27]程岳山, 张翠娟. 泰山医学院学报, **2007**,**28**(4):263-266
CHENG Y S, ZHANG C J. *Journal of Taishan Medical College*, **2007**,**28**(4):263-266

[28]Jing N, Zhou A N, Xiang Y Q, Xu Q H. *Mater. Chem. Phys.*, **2018**,**205**:480-486

[29]Jing N, Zhou A N, Xu Q H. *J. Hazard. Mater.*, **2018**,**353**:89-98